UC Riverside
BCOE Research

Title
Using PPP Information to Implement a Global Real-Time Virtual Network DGNSS Approach

Permalink
https://escholarship.org/uc/item/4sz257q9

Authors
Hu, Wang
Neupane, Ashim
Farrell, Jay A

Publication Date
2022-06-28

Peer reviewed

Using PPP Information to Implement a Global Real-Time Virtual Network DGNSS Approach

Wang Hu, Ashim Neupane, and Jay A. Farrell, *Fellow, IEEE*

Abstract—Differential GNSS (DGNSS) has been demonstrated to provide reliable, high-quality range correction information enabling real-time navigation with centimeter to sub-meter accuracy, which is required for applications such as connected and autonomous vehicles. However, DGNSS requires a local reference station near each user. For a continental or global scale implementation, this information dissemination approach would require a dense network of reference stations whose construction and maintenance would be prohibitively expensive. Precise Point Positioning (PPP) affords more flexibility as a public service for Global Navigation Satellite Systems (GNSS) receivers, but its State Space Representation (SSR) format is not supported by most receivers in the field or on the market.

This article proposes a novel Virtual Network DGNSS (VN-DGNSS) approach and an optimization algorithm that is key to its implementation. The approach capitalizes on the existing PPP infrastructure without the need for new physical reference stations. Specifically, no reference station is needed in the local vicinity of any user. By connecting to public GNSS SSR data services, a VN-DGNSS server maintains current information about satellite code bias, satellite orbit and clock, and atmospheric models. Construction of the Radio Technical Commission for Maritime Services (RTCM) Observation Space Representation (OSR) messages from this SSR information requires both the signal time-of-transmission and the satellite position at that time which are consistent with the time-of-reception for each client. This article presents an algorithm to determine these quantities. Then the VN-DGNSS computes and transmits RTCM OSR messages to user receivers. This approach achieves global dissemination coverage for real-time navigation without the need for additional local base stations near each user.

The results of real-time stationary and moving platform evaluations are included, using u-blox M8P and ZED-F9P receivers. The performance surpasses the Society of Automotive Engineering (SAE) specification (68% of horizontal error $\leqslant$ 1.5 m and vertical error $\leqslant$ 3 m) and shows significantly better horizontal performance than GNSS Open Service (OS). The moving tests also show better horizontal performance than the ZED-F9P receiver with Satellite Based Augmentation Systems (SBAS) enabled and achieve the lane-level accuracy (95% of horizontal errors less than 1 meter).

Index Terms—Differential GNSS, Precise Point Positioning, Lane-level Positioning, Virtual Base Station

I. INTRODUCTION

IMPORTANT real-time transportation applications require positioning services with high accuracy and reliability

(e.g., lane determination, lane-level queue determination, lane-specific direction guidance or traffic signal management, eco driving, speed harmonization) [1]–[4]. GNSS is a popular potential solution approach.

The GNSS OS without external correction service typically achieves 10 meters accuracy in real-time under the open sky. Specifically, GPS, Galileo, and BeiDou, respectively, provide 95% of horizontal error less than 8 m, 7.5 m, and 10 m; 95% of vertical error less than 13 m, 15 m, and 10 m [5]–[7]. This OS accuracy is not sufficient to satisfy the requirements of many Intelligent Transportation System (ITS) and Connected and Autonomous Vehicle (CAV) applications. Several references state position accuracy specifications, for instance: the Society of Automotive Engineering (SAE) specification requires 68% of horizontal error to be less than 1.5 m and vertical error to be less than 3 m [1]; and, lane-level positioning accuracy for ITS applications require 95% of horizontal error to be less than 1 m [2], [3]. Mitigation of common-mode GNSS measurement errors (e.g., satellite orbit and clock errors, hardware bias, atmospheric delay) is required to improve position accuracy in real-time navigation to achieve these specifications.

Two GNSS correction approaches have been demonstrated to effectively improve the GNSS positioning accuracy: OSR and SSR. Traditional DGNSS approaches use OSR corrections, for example, a local base station sending its measurements in an RTCM format allows correction of common-mode errors by nearby receivers. Code-measurement DGNSS can achieve 0-3 meters accuracy, while the phase-measurement DGNSS (i.e., Real-time Kinematic Positioning (RTK)), can achieve centimeter-level accuracy when the carrier phase integer ambiguities are correctly resolved (see Table 21.7 of [8]). In OSR approaches, each receiver must change its base station when its motion carries it beyond the coverage area of the current base station. PPP approaches [9] rely on correction information communicated in SSR format. Different portions of the SSR messages correct each type of common-mode error. The global accuracy of the information in the SSR messages is maintained and distributed freely by public governmental agencies, using existing worldwide networks of GNSS receivers. While most commercially available receivers do accept RTCM OSR messages, they do not currently accept RTCM SSR messages. Even after the next generations of receivers begin to accept SSR messages, there will still be numerous previously installed receivers that can only use RTCM OSR messages.

There are approaches currently available that enable correction of common-mode errors using PPP type information in commercial receivers, under limited circumstances. Com-

mercial services, such as Trimble RTX, use PPP technology to provide real-time, centimeter-level positioning worldwide. The corrections are delivered through cellular or their communication satellite. This service is only available for specific Trimble receivers at a high service cost [10] and their technical approach is not described in the open literature. SBAS services (e.g., WAAS for GPS in North America, EGNOS for Galileo in Europe, and BDSBAS for BeiDou in China) offer increased accuracy over wide-areas, approaching continental scale, for their specific GNSS system. However, there are limitations of the existing SBAS. First, many legacy receivers are not compatible with SBAS or PPP. Second, groups of nations have implemented forms of SBAS within limited geographic regions. At present, there is no globally available SBAS. Even within the area that an SBAS is specified to operate, its SBAS information is only available when that system's SBAS satellite is tracked. Third, each SBAS provides corrections to only one satellite constellation, which limits the performance robustness. For example, within North American, WAAS supplies corrections for GPS, but not for Galileo, Beido, or GLONASS. Even within North America, terrain, buildings, or foliage may limit the number of GPS satellites that are visible. Satellites from other constellations would still be available, but without corrections; therefore, accuracy will be degraded relative to the VN-DGNSS approach described herein that can provide corrections for Multi-GNSS satellites.

Existing Network DGNSS approaches also aim to overcome the limitations of local DGNSS. The Virtual Reference Station (VRS) or Virtual Base Station (VBS) approaches [11], [12] use observations from a network of reference stations. A master station virtually shifts actual observations from the reference stations to the rover site. These approaches offer wide-area coverage, determined by the extent of the reference station network. Due to the cost of installing and maintaining a reference station network over a large geographic region, existing large-scale implementations are mainly commercial and fee-based. Trimble VRS, supporting GPS and GLONASS, claims to provide centimeter-level accuracy for parts of the area of North America, Europe, and Australia [10], [13]. This service is only supported by specific Trimble receivers. OmniSTAR VBS is a GPS L1 only, code phase pseudorange solution on a global scale. It generates RTCM SC104 OSR corrections for the user specified location. This service claims that a typical 24-hour sample will show 95% with less than 1-meter horizontal error [14]. Both Trimble VRS and OmniSTAR VBS are subscription based services. Qianxun SI FindM is another sub-meter accuracy positioning service, but it is only available within China [15]. The methodology of these approaches is not reported in the open literature. These Network DGNSS approaches rely directly on receiver's measurements, not PPP information.

This paper proposes an open-source[1] that uses publicly available, real-time, PPP data and error models to construct RTCM OSR messages at the user-specified location. This approach can provide a Multi-GNSS correction service to users

globally, without cost to the user. The RTCM OSR messages that are transmitted are accepted by most receivers. In this approach, there is no need for additional *physical* reference stations. The RTCM OSR format communicates corrections in the form of an observation, which must be computationally constructed in any VN-DGNSS approach using PPP information. The computationally constructed observation requires the satellite position and time-of-transmissions for each satellite to be consistent for measurements at a specified time at the user-specified location. Section III presents an optimization algorithm that solves this problem. Section IV describes the use of PPP information to construct the observation. Section V discusses the client-server architecture and PPP information sources. The currently implemented system is single frequency (i.e., GPS L1, Galileo E1, and BeiDou B1) and pseudorange only. Section VI describes experimental results. Our initial tests demonstrate the feasibility of improving positioning accuracy to surpass the SAE specification. The moving tests also achieve lane-level accuracy requirements. Its extension to carrier phase and multi-frequency are discussed in Sections IV-E and VIII, respectively.

II. GNSS Pseudorange Observations

Each GNSS constellation $\mathbf{S}$, that uses Code Division Multiple Access (CDMA)[2], transmits signals using f carrier frequencies. The code (pseudorange) observation from satellite s tracked by receiver r at the GNSS receiver time t_r is modeled as (see Chap. 21 of [8])

$$\left. \begin{array}{l} \rho_{f,r}^s(t_r) = R\left(\mathbf{P}_r(t_r), \hat{\mathbf{P}}^s(t^s)\right) + E_r^s(t^s) - c\,dt^s + cB_f^s \\ \qquad + c\,dt_r + c\,d_r^S + T_r^s + I_{f,r}^s + M_{f,r}^s + \eta_{f,r}^s, \end{array} \right\} \quad (1)$$

where $\mathbf{P}_r$ denotes the receiver antenna position, $\hat{\mathbf{P}}^s$ denotes the satellite position computed using the satellite navigation message, while t^s denotes the time when the signal was transmitted. The symbols dt^s and $\hat{dt}^s$, and other important symbols, are defined as in Table I.

Both $\mathbf{P}_r$ and $\hat{\mathbf{P}}^s$ are defined in the Earth-Centered Earth-Fixed (ECEF) frame. Because the ECEF frame is rotating, the range quantity in Eqn. (1) must be interpreted carefully, as the ECEF frame is oriented differently at times t^s and t_r. Let E_r and E_s represent the ECEF frames at time t_r and t_s respectively. The rotation matrix $R_{E_s}^{E_r}$ rotates vectors from their representation in frame E_s to E_r Therefore,

$$R(\mathbf{P}_r(t_r), \hat{\mathbf{P}}^s(t^s)) = \|\mathbf{P}_r(t_r) - \mathbf{R}_{E_s}^{E_r}\,\hat{\mathbf{P}}^s(t^s)\|.$$

Alternatively, this range can be computed by the well known Sagnac correction:

$$R(\mathbf{P}_r(t_r), \hat{\mathbf{P}}^s(t^s)) = \|\mathbf{P}_r(t_r) - \hat{\mathbf{P}}^s(t^s)\| + \frac{\omega_{ie}}{c}(xb - ay), \quad (2)$$

TABLE I: Notation definitions.

ω_{ie}:	Earth rotational rate (rad/s),
c:	Speed of light (m/s),
E_r^s:	Satellite range ephemeris error (m),
δt^s:	Satellite clock model error, $\delta t^s = (\hat{d}t^s - dt^s)$, (s),
$\hat{d}t^s$:	Broadcast satellite clock correction (s),
dt^s:	Satellite clock bias (s),
B_f^s:	Satellite code hardware bias (s),
dt_r:	Receiver clock error (s),
d_r^S:	Receiver code hardware bias for system S (s),
T_r^s:	Tropospheric delay (m),
$I_{f,r}^s$:	Ionospheric delay for f frequency (m),
$\eta_{f,r}^s$:	Random code measurement noise (m),
$M_{f,r}^s$:	Multipath error (m).

TABLE II: GNSS range measurement error magnitudes.

Error Source	Typical Magnitude	Reference
Satellite range ephemeris	~ 2 m	[23]
Satellite clock	~ 5 ns	[23]
Satellite code bias	~ 20 ns	[24]–[26]
Troposphere delay	~ 2.3 m	[27]
Ionosphere delay	< 30 m	Sec. 25.2 in [8]
Code multipath	< 3 m	Sec. 8.4.7 in [28]
Measurement noise	< 1 mm	Sec. 19.7.1 in [8]

where $\mathbf{P}^s = [x, y, z]^T$ and $\mathbf{P}_r = [a, b, c]^T$. The accuracy of the Sagnac correction is analyzed in [22] where it is shown to be accurate to 10^{-6} m.

The goal of the state estimator using GNSS is to accurately estimate the state vector, which will include the position $\mathbf{P}_r$, the receiver hardware bias for each system d_r^S, and the receiver clock error δt_r. The model for $\hat{d}t^s$, which includes a polynomial and a relativistic correction, can be found in the Interface Control Document (ICD) of each constellation (Sec. 20.3.3.3.3.1 in [16], Sec. 5.1.4 in [17], and Sec. 7.4 in [18]). The remaining satellite clock model error is $\delta t^s = (\hat{d}t^s - dt^s)$.

The error terms of the measurement model of Eqn. (1) can be classified into two categories:

- Common-mode errors are essentially the same for all receivers in a local vicinity. These include: satellite range ephemeris and clock model errors, satellite code hardware bias, and atmospheric (ionospheric and tropospheric) error.
- Non-common-mode errors are different for each receiver. These include: code multipath error and random code measurement noise.

These errors significantly affect the positioning accuracy. The typical error magnitudes are summarized in Table. II.

There are three standard methods to decrease the effects of GNSS measurement errors. First, for GNSS OS approaches (i.e., GPS standard positioning service (GPS SPS), Galileo OS, and Beidou OS), the Single-frequency Point Positioning (SPP) solution only uses a prior troposphere model and an ionosphere model with parameters from the navigation message to reduce the atmospheric errors (Chap. 21 of [8]). GNSS OS approaches are still affected by satellite biases, residual ephemeris and clock errors. Second, for OSR approaches using the RTCM standard, GNSS measurements from a receiver at a known

location near to the user receiver are communicated to the user receiver, which forms differential measurements that are essentially free from common-mode errors [9]. Essentially all receivers can accept RTCM OSR messages. Third, SSR approaches communicate correction information for each portion of the common-mode range errors separately [24], [29] from an on-line data source to the receiver. At present, few receivers are available that accept SSR correction information. Even as more receivers become available that accept SSR correction information, legacy receivers will require correction information in OSR format. This paper presents a method to compute OSR format differential information from on-line SSR information, which alleviates the need for local base stations. The RTCM format for communicating OSR correction information is as a measurement.

Considering Eqn. (1) from the perspective of constructing an RTCM OSR message using SSR data for a known virtual base antenna position $\mathbf{P}_b$. First, the base station receiver clock error $\Delta t_b^S = dt_b + d_b^S$ is not important for positioning applications. This error will only affect the estimated rover clock error, since it is identical for all code measurements of constellation S. Therefore, for the virtual base station, both dt_b and d_b^S are set to zero. Second, the multipath and receiver terms $(M_{f,b}^s + \eta_{f,b}^s)$ are non-common-mode errors and should not be included. Therefore, the desired code measurement to send as an RTCM OSR message is modeled as

$$\left.\begin{aligned}
\rho_{f,b}^s(t_b) = {}& R\left(\mathbf{P}_b, \hat{\mathbf{P}}^s(t^s)\right) \\
& + \hat{E}_b^s(t^s) - c\left(\hat{d}t^s - \delta\hat{t}^s\right) + c\hat{B}_f^s \quad + \hat{T}_b^s + \hat{I}_{f,b}^s.
\end{aligned}\right\} \quad (3)$$

The server (i.e., VRS) transmits RTCM 3.X messages to the receiver which include the virtual base station position $\mathbf{P}_b$ and time t_b, and the computed code measurements $\rho_{f,b}^s(t_b)$. The code measurement construction can be decomposed into two parts. Section III will discuss the computation of $R\left(\mathbf{P}_b, \hat{\mathbf{P}}^s(t^s)\right)$, which hinges on computation of satellite position $\hat{\mathbf{P}}^s(t^s)$. Section IV will discuss the computation of the common-mode corrections in the second line of Eqn. (3) from the SSR data.

III. SATELLITE POSITION, RANGE, AND TIME-OF-TRANSMISSION

The purpose of this section is to compute the term $R\left(\mathbf{P}_b, \hat{\mathbf{P}}^s(t^s)\right)$ in the first line of Eqn. (3) when the base location $\mathbf{P}_b$ and measurement time t_b are given. This computation must determine the location $\hat{\mathbf{P}}^s(t^s)$ for which the signal received from satellite s transmitted at time t^s would be received at time t_b by a virtual receiver at location $\mathbf{P}_b$. These computations will neglect the common-mode errors, whose effect is analyzed in Section III-B.

For a signal pseudo-transmit-time $\hat{t}^s$, the ICD provides equations and the broadcast navigation message provides data to compute the satellite clock offset $\hat{d}t^s(\hat{t}^s)$, satellite position $\hat{\mathbf{P}}^s(\bar{t}^s)$ and satellite velocity $\hat{\mathbf{V}}^s(\bar{t}^s)$, where $\bar{t}^s = (t_b - t_p^s - \hat{d}t^s)$ is the time-of-signal-transmission corrected by the navigation satellite clock error model from the ICD.

A. Algorithm Definition

The range between the satellite and virtual base antennae can be computed in two ways:

$$R\left(\mathbf{P}_b, \hat{\mathbf{P}}^s(t_b - t_p^s - \hat{d}t^s)\right) \text{ and } c\ (t_p^s + \hat{d}t^s) \quad (4)$$

Algorithm 1 adjusts the (uncorrected) propagation time t_p^s to compute the satellite position $\hat{\mathbf{P}}^s(\bar{t}^s)$ at the corrected time of transmission $\bar{t}^s$ by minimizing the error between the two range equations:

$$F(t_p^s : \mathbf{P}_b, t_b) = R\left(\mathbf{P}_b, \hat{\mathbf{P}}^s(t_b - t_p^s - \hat{d}t^s)\right) - c\ (t_p^s + \hat{d}t^s). \quad (5)$$

The quantity $t_g^s = t_p^s + \hat{d}t^s$ is the geometric travel time. The notation $F(t_p^s : \mathbf{P}_b, t_b)$ means that t_p^s is the argument and $\mathbf{P}_b$ and t_b are known parameters.

The optimization is implemented using numeric search. Step 1 initializes the propagation time to $t_p^s = 0.067$ seconds because GNSS satellites are approximately 20,000 km from the Earth surface. Step 2 declares a parameter to store the last value of t_p^s. Step 3 starts the while loop which terminates when $|t_p^- - t_p^s|$ is small. Step 4 computes the pseudo-transmit time $\hat{t}^s$, which is used in Step 5 to compute the satellite clock correction $\hat{d}t^s(\hat{t}^s)$, and the position $\hat{\mathbf{P}}^s(\bar{t}^s)$ and velocity $\hat{\mathbf{V}}^s(\bar{t}^s)$. The ICD models [16]–[18] are represented by the function $f(\hat{t}^s, \boldsymbol{\theta}_e^s)$ where $\boldsymbol{\theta}_e^s$ are the broadcast ephemeris and clock correction parameters. Steps 6 - 9 compute the two ranges and the range error for the current value of t_p^s. Step 10 computes the partial derivative of the cost with respect to the t_p^s

$$\frac{\partial F}{\partial t_p^s} = -\left(\mathbf{1}_b^s \cdot \hat{\mathbf{V}}^s(\bar{t}^s) + c\right)\left(1 - a_1 - 2a_2\left(\hat{t}^s - t_{oc}\right)\right), \quad (6)$$

where a_1, a_2, and t_{oc} are the clock model parameters from the navigation message. Step 11 stores the t_p^s to t_p^- before updating t_p^s Step 12 implements Newton's Zero Finding Algorithm to optimize t_p^s to minimize the square of the error defined in Eqn. (5). Step 14 computes satellite transmission time $\bar{t}^s$ which will be used as t^s in the SSR clock product of Section IV-A.

For the input receiver time t_b and base station location $\mathbf{P}_b$, this optimization process provides the broadcast clock correction $\hat{d}t^s(\hat{t}^s)$ and the satellite location $\hat{\mathbf{P}}^s(\bar{t}^s)$ at the corrected time of transmission. These enable computation of $R\left(\mathbf{P}_b, \hat{\mathbf{P}}^s(\bar{t}^s)\right)$ as required for the RTCM OSR measurement defined in Eqn. (3).

B. Effect of Common Mode Errors

At the user receiver, residual measurements are formed for both the base and user receiver measurements. For the base measurements, the available information is t_b and $\rho_{f,b}^s(t_b)$. The user receiver computes the time of satellite transmission as

$$\tilde{t}^s = t_b - \frac{1}{c}\rho_{f,b}^s(t_b),$$

where $\tilde{t}_p^s = \frac{1}{c}\rho_{f,b}^s(t_b)$ is the measured propagation time. Because the measurement of $\rho_{f,b}^s(t_b)$ includes errors, as modeled in Eqn. (1), the measured and actual values of the transmit time are related according to

$$\tilde{t}^s = \bar{t}^s - e_b^s,$$

Algorithm 1 Satellite Position Estimation

Input: $\mathbf{P}_b$, t_b.
Output: $\hat{\mathbf{P}}^s(t^s)$, $\hat{V}^s(t^s)$, $\hat{d}t^s$ and t^s.
1: $t_p^s = 0.067$;　　　　　　// Initialize the propagation time
2: $t_p^- = 0$;　　　　　　　// Initialize previous value to 0
3: **while** $|t_p^- - t_p^s| > 10^{-11}$ **do**
4:　　$\hat{t}^s = t_b - t_p^s$;　　　　　　// Pseudo-transmit-time
5:　　$[\hat{\mathbf{P}}^s(\bar{t}^s), \hat{\mathbf{V}}^s(\bar{t}^s), \hat{d}t^s(\hat{t}^s)] = f(\hat{t}^s, \boldsymbol{\theta}_e^s)$;　　// ICD models
6:　　$R_1 = R(\mathbf{P}_b, \hat{\mathbf{P}}^s(\bar{t}^s))$　　　// Range based on position
7:　　$t_g^s = t_p^s + \hat{d}t^s(\hat{t}^s)$　　　// See definition in Eqn. (5)
8:　　$R_2 = c \cdot t_g^s$　　// Range based on geometric travel time
9:　　$F = R_1 - R_2$;　　　　　　　// Eqn. (5)
10:　　$dF = -\left(\frac{\hat{\mathbf{V}}^s(\bar{t}^s) \cdot (\hat{\mathbf{P}}^s - \mathbf{P}_b)}{R_1} + c\right)\left(1 - \frac{\partial}{\partial t_p^s}\hat{d}t^s(\hat{t}^s)\right)$;　// Eqn. (6)
11:　　$t_p^- = t_p^s$;　　　　　　　// save the previous value
12:　　$t_p^s = t_p^s - \frac{F}{dF}$;　　// Newton's Zero Finding Algorithm
13: **end while**
14: $\bar{t}^s = t_b - t_p^s - \hat{d}t^s(\hat{t}^s)$.　　// Transmit time by the satellite clock

---

where e_b^s denotes both common-mode and non-common-mode errors scaled to units of time (i.e., $|e_b^s| \leq 200$ ns). The error e_b^s is neglected in the algorithm of the previous section. This section analyzes the effect of this decision on the satellite position and its range from the base.

The algorithm computes $\mathbf{P}^s(\bar{t}^s)$ when it should have computed $\mathbf{P}^s(\bar{t}^s - e_b^s)$. Consider the Taylor series expansion:

$$\mathbf{P}^s(\bar{t}^s - e_b^s) = \mathbf{P}^s(\bar{t}^s) - \left.\frac{\partial}{\partial t}\mathbf{P}^s(t)\right|_{t=\bar{t}^s} e_b^s \quad (7)$$

$$= \mathbf{P}^s(\bar{t}^s) - \mathbf{V}^s(\bar{t}^s) e_b^s \quad (8)$$

Therefore, because the satellite speed is about 4,000 m/s and $|e_b^s| \leq 2 \times 10^{-7}$, the effect of neglecting e_b^s on the satellite position calculation is less than one millimeter.

IV. COMMON-MODE ERROR CALCULATIONS

This section focuses on the use of SSR data to compute the common mode error terms in the second line of Eqn. (3). These calculations will depend on the given base position P_b which is considered as known to the server and the satellite position $\hat{P}^s(t^s)$ which is computed as described in Section III.

A. Satellite Orbit and Clock Corrections

The SSR data streams provide orbit and clock products to correct the satellite position $\hat{P}^s(t^s)$ and clock error $\delta t^s(t^s)$ at the transmit time t^s.

The orbit correction consists of orbit $\delta \mathbf{O} = [\delta O_r, \delta O_a, \delta O_c]^T$ and rate $\delta \dot{\mathbf{O}} = [\delta \dot{O}_r, \delta \dot{O}_a, \delta \dot{O}_c]^T$ corrections along with a reference time t_o. These define radial (δO_r, $\delta \dot{O}_r$), along-track (δO_a, $\delta \dot{O}_a$) and cross-track (δO_c, $\delta \dot{O}_c$) components. The calculation of the corrected satellite position $\tilde{\mathbf{P}}^s(t^s)$ from the SSR orbit correction parameters is presented in Sec. 4.1 of [30] (see [9] for the calculation using the notation of this paper). The satellite range ephemeris error E_r^s is computed as

$$E_b^s = R(\mathbf{P}_b(t_b), \tilde{\mathbf{P}}^s(t^s)) - R(\mathbf{P}_b(t_b), \hat{\mathbf{P}}^s(t^s)). \quad (9)$$

The satellite clock correction is transmitted as three polynomial parameters (C_i^s, $i = 0, 1, 2$) with a corresponding reference time t_c^s. The clock correction for satellite s at transmit time t^s is:

$$\delta C^s(t^s) = C_0^s + C_1^s(t^s - t_c^s) + C_2^s(t^s - t_c^s) \quad \text{meters.} \quad (10)$$

To be consistent with Eqn. (4) in [31], the correction of satellite clock error $\delta \hat{t}^s$ (i.e., correction of the broadcast clock error) is

$$\delta \hat{t}^s(t^s) = -\frac{\delta C^s(t^s)}{c} \quad \text{seconds.} \quad (11)$$

B. Satellite Hardware Bias

Satellite hardware biases have various causes such as analog group delays in the front-end and digital delays. They are normally very stable over time (i.e., constant over at least a single day) [32]. GNSS OS users can apply the Timing Goup Delay (TGD) to roughly correct the hardware bias [33]. The TGD is computed by the GNSS control segment and broadcast in the navigation message for GNSS OS users.

To attain higher accuracy, SSR operations may use either Differential Code Bias (DCB) or Observable-specific Code Biases (OSB) corrections, as defined in the SINEX standard [34]. For the OSB product, let the symbol $B_{(\mathbf{S},T)}$ to denote the correction for observation type T of constellation $\mathbf{S}$ (e.g., T could be the C1C observation type with S denoting GPS). The $B_{(\mathbf{S},T)}$ correction products are available in SSR format from sources such as Chinese Academy of Sciences (CAS) GIPP [35]. For SSR users, the observation $O_{(\mathbf{S},T)}$ is corrected by $B_{(\mathbf{S},T)}$ as

$$O'_{(\mathbf{S},T)} = O_{(\mathbf{S},T)} - B_{(\mathbf{S},T)} \quad (12)$$

to produce the OSB-corrected observation $O'_{(\mathbf{S},T)}$.

For the OSR measurement in Eqn. (3),

$$\hat{B}_f^s = B_{(\mathbf{S},T)}. \quad (13)$$

C. Global Troposphere Model

The troposphere is the lowest layer of the atmosphere, extending to about 60 kilometers above the Earth's surface. In this layer, the speed of light is slower than in a vacuum, so the radio signal is delayed. The delay is affected by numerous meteorological parameters relevant within the vicinity of the receiver, e.g., temperature, pressure, and relative humidity. Numerous tropospheric delay correction models have been introduced [36]–[38]. These models avoid the need for real-time measurement of the meteorological parameters.

IGGtrop [37] is one such global empirical model. It computes the slant troposphere delay T_r^s as:

$$T_b^s(E, t) = M(E) \, T_z(t) \quad (14)$$

where E is the satellite elevation angle at the rover position;

$$M(E) = 1.001 \left(0.002001 + sin^2(E) \right)^{-\frac{1}{2}} \quad$$

is the mapping function [39] for converting the Zenith Troposphere Delay (ZTD) to the slant tropospheric delay; and, $T_z(t)$

is the ZTD (i.e., tropospheric delay in the zenith direction above the receiver). IGGtrop computes $T_z(t)$ as

$$T_z(t) = a_0 + a_1 \cos(\gamma t) + a_2 \sin(\gamma t) \quad (15)$$
$$+ a_3 \cos(2\gamma t) + a_4 \sin(2\gamma t)$$

where $\gamma = (2\pi/365.25)$ and the units of t are real-valued days of the year. The coefficients a_0, (a_1, a_2) and (a_3, a_4) model the mean value, the annual variation and the semi-annual variation in ZTD, respectively. IGGtrop defines these parameters on a 3-D grid in latitude, longitude, and altitude around the globe. This enables interpolation of the ZTD at a receiver position to achieve 3.86cm root-mean-square error and -0.46cm average bias; however, it requires 666k parameters to implement a global grid.

There are several variants of IGGtrop [37], [40], [41]. The trade-offs between them related to the required number of parameters and the resulting accuracy. The VN-DGNSS server currently implements the IGGtrop_SH variant [41]. This approach computes the coefficients a_0, a_1, a_2, a_3, a_4 for Eqn. (15) using the empirical model:

$$a_0(h) = exp\left(\sum_{i=0}^{m} \alpha_i h^i \right), \quad (16)$$

$$a_j(h) = \sum_{i=0}^{5} \beta_{ji} h^i + c, \ \forall j \in \{1, 2, 3, 4\}, \quad (17)$$

where h is the altitude of the receiver. In Eqn. (16), the parameter m is a function of the receiver latitude (see Section III in [41]). The coefficients α_j and β_{ji} are defined on a 2-D grid in latitude and longitude. These values were provided by the first author of [41]. The value of $T_z(t)$ is computed at the four nearest points on the 2-D grid and interpolate to compute its value at the receiver position.

D. Ionosphere Model

The ionosphere is the ionized zone of the atmosphere containing free electrons and positively charged ions. It ranges from about 50 km to 1000 km above the Earth surface. Electromagnetic signals are refracted in the ionosphere (Sec. 6.3 in [8]). It is a dispersive medium that impacts different frequencies, and the carrier and modulating signals, differently.

In GNSS OS processes, the dual-frequency user is able to form ionosphere-free combinations or estimate ionospheric delay using two measurements tracked for two frequencies from one satellite. The single-frequency users apply a prior model (i.e., Klobuchar for GPS and BeiDou [16], [18], [42], NeQuick for Galileo [17], [43]) using ionosphere parameters from the navigation message to reduce the ionosphere delay by about 50% Root Mean Square (RMS) [44], [45]. Real-time, single-frequency, PPP users compensate the ionosphere delay by processing ionosphere products. The VN-DGNSS server includes two possible ionospheric products. Both compute the ionosphere delay for the code measurement on frequency f by

$$I_{f,b}^s = \frac{40.3}{f^2} STEC \ 10^{16}. \quad (18)$$

Each has a different method for computing the Slant Total Electron Content (STEC) from a model of the Vertical Total

Electron Content (VTEC). VTEC is computed at the Ionosphere Pierce Point (IPP), which is computed from the virtual base location $\mathbf{P}_b$ and the computed satellite location $\hat{\mathbf{P}}^s(\bar{t}^s)$.

SSR VTEC-SH: The agencies listed in Table III provide real-time VTEC SSR products that have global applicability. In the RTCM Version 3 standard [46], the real-time VTEC SSR message provides the parameters for a Spherical Harmonic (SH) expansion with degree of the expansion N, order of the expansion M, and coefficients $C_{n,m}$ and $S_{n,m}$ for $n = 0,\ldots,N$ and $m = 0,\ldots,M$. For a single-layer model, the VTEC model at the IPP is [30], [47]

$$VTEC(\phi_{PP}, \lambda_{PP}) = \sum_{n=0}^{N} \sum_{m=0}^{min(n,M)} P_{n,m}(\sin(\phi_{PP})) \quad (19)$$

$$\cdot (C_{n,m} \cos(m\lambda_S) + S_{n,m} \sin(m\lambda_S)) \quad (20)$$

where $P_{n,m}()$ is the normalized associated Legendre function, $(\phi_{PP}, \lambda_{PP})$ are the geocentric latitude and longitude of the IPP, and λ_S is computed by

$$\lambda_S = (\lambda_{PP} + (t - 50400) * \pi/43200)\, modulo\,(2\pi) \quad (21)$$

where t is the SSR epoch time of computation, modulo 86400 seconds.

The STEC is computed from VTEC using

$$STEC = \frac{VTEC}{sin(E + \phi_{PP})} \quad (22)$$

where E is the elevation angle of the satellite at the rover position.

TABLE III: Public real-time global ionosphere VTEC modeling services providing RTCM VTEC message. Each has NTRIP caster ID: 'products.igs-ip.net:2101'.

Agency	SH degree	Mount point	References
CAS	15	SSRA00CAS0	[48]
CNES	12	SSRA00CNE0	[49]

US-TEC: For North America users, the National Oceanic and Atmospheric Administration (NOAA) provides the real-time US Total Electron Content (US-TEC) product for public usage [50]. US-TEC provides VTEC values in a uniform grid of point locations with 1 degree resolution in latitude and longitude. The official website [51] states that the normal update interval is 15 minutes, typically with 28 minutes latency[3].

The VTEC at the IPP (within the geographical extent of the grid points) is computed as a linear function of the values at grid points. The VN-DGNSS server uses distance weighted spatial interpolation [52], [53]:

$$VTEC(IPP) = \mathbf{w}(IPP)\, \mathbf{I}^G, \quad (23)$$

where $\mathbf{w}(IPP)$ is a vector of weights. Both $\mathbf{w}(IPP)$ and $\mathbf{I}^G$ are vectors with K components. The k-th element w_k of the weighting vector determines the amount that a VTEC value

$[\mathbf{I}^G]_k$ at the k-th grid point IPP_k contributes to the value of Total Electron Content (TEC) at the desired IPP.

The vector $\mathbf{w}(IPP) = [w_1,\ldots,w_K]$ satisfies the following constraints:

1) $\sum_{i=1}^{K} w_k = 1$, so that Eqn. (23) interpolates the value for VTEC from the grid points.
2) the k-th element w_k should decrease smoothly as $d_k = \|IPP - IPP_k\|$ increases. This results in a smooth interpolation between the grid point values.

The approach herein uses at most four nonzero weights. If $IPP = IPP_k$ for some k, then $w_k = 1$ and all remaining values of $\mathbf{w}(IPP)$ are zero. Otherwise, the IPP is between four grid points. In this case, we define $a \in \Re^K$ such that $a_k = 1/d_k$ for those four corner grid points, noting that a_k is finite because $d_k \neq 0$. All the remaining elements of $\mathbf{a}$ are zero. Then, the components of $\mathbf{w}(IPP)$ are defined as $w_k = \frac{a_k}{\sum_{i=1}^{K} a_i}$.

Spatial interpolation provides the VTEC at the IPP. The STEC is computed as [53]:

$$STEC = F(E)VTEC(IPP). \quad (24)$$

where $F(E)$ is the ionospheric obliquity factor defined as

$$F(E) = \frac{1}{\sqrt{1 - \left[\frac{r_e \cos(E)}{r_e + h_m}\right]^2}}, \quad (25)$$

where r_e is the average radius of the earth, and h_m is the height of the maximum electron density (assumed herein to be 350 km).

E. Discussion

The present server approach is designed for pseudorange positioning, using manufacturer software. It was not designed for carrier phase (i.e., RTK) positioning for a few reasons. First, the project supporting this research was focused on single-frequency approaches, while practical PPP-RTK requires a multi-frequency solution to allow widelane implementations (Sec. 21.4.5 in [8]). Second, the use of a virtual base instead of a physical base means that various of the common-mode errors (e.g., satellite hardware biases) are not accounted for (in the corrections) to the extent required for the double-difference operations to result in 'integer' ambiguities [54].

V. VN-DGNSS SERVER-CLIENT SYSTEM DESIGN

This section describes the software implementation for a publicly available, open-source, client/server VN-DGNSS implementation with global coverage. The server receives real-time information in SSR format and provides each client with virtual base station RTCM OSR formatted messages applicable to their local vicinity for BeiDou B1, GALILEO E1, and GPS L1. This approach eliminates the need for the client to have physical access to a local reference station.
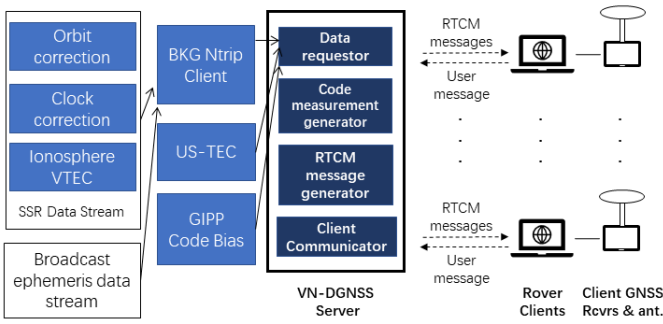
---

[3]During the period from late 2020 through the middle of 2021, the latency was over 24 hours; therefore, although US-TEC is included in the software distribution, it was not used in the demonstration experiments described in Section VI.

Fig. 1: VN-DGNSS server-client architecture

A. System Architecture

Fig. 1 displays the VN-DGNSS client/server framework. The VN-DGNSS server includes four fundamental components.

- The *data requestor* establishes communications with on-line sources to maintain real-time SSR data. The BKG NTRIP Client (BNC) [55] provides broadcast ephemeris for each satellite system, Multi-GNSS SSR orbit and clock corrections, and SSR VTEC information (see Table III). US-TEC products are included as an option for US clients. CAS GIPP provides code bias products [35]. Because the IGGtrop_SH parameters are static, they are loaded at run-time and do not require real-time communications.
- The *code measurement generator* constructs the code measurements, for the virtual base position $\mathbf{P}_b$ requested by the client, using Eqn. (3) for GPS L1, Galileo E1 and Beidou B1. The range is computed as described in Section III. The correction terms in the second line of Eqn. (3) are computed using the models discussed in Section IV.
- The *RTCM message generator* creates RTCM message type 1004 and MSM4 message types: 1074 for GPS, 1094 for Galileo, 1124 for BeiDou. The RTCM 1004 message communicates the virtual reference station position $\mathbf{P}_b$. The RTCM MSM4 message includes the code measurements constructed by the code measurement generator at integer epoch times t_b (i.e., 1.0 Hertz), along with the observation type and Signal-to-Noise Ratio (SNR)[4].
- The *client communicator* receives requests from, then establishes and maintains TCP connections with clients. In addition to its internet address, the client sends its (desired) virtual reference station position $\mathbf{P}_b$, and the GNSS constellations and the observation types for which the client desires RTCM messages. Clients that are moving can update their desired virtual reference station position as necessary to keep it within a reasonable distance (e.g., 20 km) of their location.

Some portions of the VN-DGNSS (e.g., code measurement generator, RTCM message generator) are modifications of open-source functions in RTKLIB [56], [57] and BNC [55].

B. Implementation Strategies

Details and choices required for the VN-DGNSS server implementation are described below.

1) Table III list the two agencies that currently stream SSR Multi-GNSS corrections and global VTEC SH parameters using RTCM messages through NTRIP. Both are available through the server.
2) The real-time orbit and clock corrections are applicable to a specific Issue Of Data (IOD) ephemeris. GPS and Galileo ephemeris provides the IOD number for each satellite. The Beidou IOD depends on the agency providing the data. The two agencies in Table III both share the same methodology:

$$BeiDou\ IOD = ((int)toe/720)\ modulo\ 240,$$

where *toe* is the time-of-ephemeris in the BeiDou navigation message [58].
3) The multi-GNSS OSB product provided by CAS [35] is referred to as GIPP. The GIPP code bias data can be downloaded from ftp://ftp.gipp.org.cn/product/dcb/daybias/. They are updated with a period of one day update and latency of 1-5 days. The two agencies listed in Table III also provide code biases through NTRIP; however, they do not provide bias estimates for all observation types required for the experiments.
4) The SSR data has two types: Antenna Phase Centre (APC) and Center of Mass (COM). The broadcast ephemeris is referred to the satellite's APC; therefore, the selected SSR data stream for orbit corrections must also reference to the APC, not COM.

VI. EXPERIMENTAL PERFORMANCE ANALYSIS

The VN-DGNSS evaluation in this section includes data from both stationary and moving platforms. This section describes the receiver hardware and configurations, virtual network data sources, metrics, and experimental results.

A. Experiment Schedule

Results from three experiments are included herein[5] from one stationary test and two moving tests.

The *stationary* test used a dual-band antenna (Trimble ACCG5ANT_2AT1) located on the roof of Winston Chung Hall at University of California-Riverside (UCR). The ground truth location of this antenna are known to centimeter accuracy from prior Online Positioning User Service (OPUS) survey results. VN-GNSS position estimates from the receiver are compared against that *ground truth* location.

For the *moving platform* experiments, a u-blox antenna is mounted on the roof of a car. Using a signal splitter, that antenna is connected to 4 receivers for each experiment. One u-blox M8P receiver is used to determine an independent *ground truth* trajectory for the time-varying antenna position. This receiver was communicating with a nearby base station

---

[4]In the current implementation, the server computes the SNR as $floor(\frac{A \cdot E}{\pi}) + \underline{S}$, where E is the satellite elevation in radians, $\underline{S}$ is the minimum SNR, and A is a coefficient that determines the maximum SNR.

[5]Additional information about the results of the experiments are described in the document 'test_data/Experiment_Support_Doc /support_doc.pdf' at the GitHub repository defined in Footnote 1).

and performing carrier-phase, integer-fixed RTK to achieve centimeter accuracy. The configurations of the remaining 3 receivers for each moving test are discussed in Section VI-F using the experiment labels from Table 5. The vehicle was driven in the urban area near UCR that had a relatively clear view of the sky. The duration of each data accumulation experiment was about 1 hr.

B. GNSS Hardware and Configuration Descriptions

The experiments used 5 low-cost receivers, each compatible with RTCM OSR messages. The text below describes and Table IV summarizes the 6 experimental configurations that are compared. The acronym VN is used to indicate VN-DGNSS.

Two u-blox M8P receivers were used. Each M8P is capable of tracking GPS, GLONASS, and Beidou satellites. VN-DGNSS does not currently incorporate GLONASS corrections, so GLONASS was disabled. With the current firmware (version 3.01 HPG 1.40), for Beidou, the M8P will use the RTCM corrections only if available for both code and phase; therefore, because VN-DGNSS does not currently provide phase measurements, the BeiDou measurements were disabled. Therefore, only GPS measurements were used with the M8P.

SF GPS SPS: An M8P was configured for Standard Positioning Service (SPS)[6] without any external correction sources, just the standard tropospheric and ionospheric models.

SF GPS VN: An M8P connects to the VN-DGNSS client to receive real-time RTCM OSR corrections.

Three u-blox ZED-F9P receivers were used. Each F9P is a dual-frequency receiver compatible with Multi-GNSS. GPS, Galileo, and BeiDou are used herein. It used Single Frequency (SF) operation when connected to a single band antenna or Dual Frequency (DF) operation when connected to a dual band antenna.

SF GNSS OS: An F9P was configured to operate in SF OS mode (i.e., SBAS disabled and no VN-DGNSS).

DF GNSS OS: An F9P is configured to operate in DF OS mode (i.e., SBAS disabled and no VN-DGNSS).

SF GNSS VN: An F9P is configured to use SF RTCM OSR messages through the VN-DGNSS client. When the client connects to the server (typically within about one second), the F9P switches to DGNSS mode.

F9P SBAS: An F9P was configured with SBAS enabled. Because the experiments occurred in California, they were within the Wide Area Augmentation System (WAAS) coverage area, allowing differential operation for GPS. The F9P typically requires a few minutes to start tracking a WAAS augmentation satellite, at which time it switches to Differential Global Positioning System (DGPS) mode and process only the L1 measurements. The GALILEO and BeiDou satellite measurements were tracked and used by the receivers in OS mode.

[6]For GPS, the open service is usually stated as SPS [5], which we use in the experiment label. Columns 2-4 of Table IV use the acronym OS instead of SPS for consistency in those columns.

TABLE IV: Descriptions of experimental configurations.

Experiment label	GNSS Systems Used			SBAS	Receiver
	GPS	GALILEO	BeiDou		
SF GPS SPS	OS	None	Disable	None	M8P
SF GPS VN	VN	None	Disable	None	M8P
SF GNSS OS	OS	OS	OS	Off	ZED-F9P
DF GNSS OS	OS	OS	OS	Off	ZED-F9P
SF GNSS VN	VN	VN	VN	Off	ZED-F9P
F9P SBAS	SBAS	OS	OS	WAAS	ZED-F9P

All receivers report their computed position every 1 second using the manufacturer algorithms. The elevation angle cutoff for all the receivers was $15°$.

C. Data Choices

Because the accuracy assessments for the real-time VTEC products [47] and for the orbit and clock products [59] indicate that Centre national d'études spatiales (CNES) has slightly better performance than CAS, we select CNES as the data source in these experiments. The reason why US-TEC was not used is stated in Footnote 3.

Table V summarizes the predicted error statistics based on the following articles: CNES real-time orbit and clock products [59]; GIPP OSB [35], [60]; IGGtrop_SH [41]; CNES VTEC [47]; along with the non-common mode errors. The VTEC errors are frequency dependent; therefore, they are slightly different for each satellite systems. The IGGtrop_SH RMS error is the same for all satellite systems because the model is for properties of the environment that are independent of frequency and of the satellite system. Based on the information in this table, multipath is the dominant remaining error source.

D. Metrics

The metrics for analyzing position error will include:
- ECEF 3-D error norm : $\|\delta \mathbf{P}^e\|$ with $\delta \mathbf{P}^e = \hat{\mathbf{P}}^e - \mathbf{P}^e$;
- Horizontal error: $HE = \sqrt{(\delta \mathbf{P}_N^g)^2 + (\delta \mathbf{P}_E^g)^2}$;
- Vertical error: $VE = |\delta \mathbf{P}_D^g|$.

The notation in these expressions is as follows. The symbol $\mathbf{P}$ denotes the ground truth position; and, $\hat{\mathbf{P}}$ denotes the position estimated by the receiver. The superscript denotes the frame-of-reference: e for ECEF and g for local tangent frame. Vectors are transformed between frames using $\delta \mathbf{P}^g = \mathbf{R}_e^g \, \delta \mathbf{P}^e$, where the symbol $\mathbf{R}_e^g$ represents the rotation matrix from the ECEF frame to the local North, East and Down (NED) frame (see

TABLE V: VN-DGNSS ranging errors.

Error	GPS (L1)	Galileo (E1)	BeiDou (B1)
CNES Orbit 3D (cm) RMS	2.88	4.42	14.54
CNES Clock (ns) RMS	0.45	0.39	3.00
CAS GIPP (ns) RMS	0.06	0.15	1.0
IGGtrop_SH (cm) RMS	3.86	3.86	3.86
CNES VTEC (cm) RMS	55.21	55.21	56.22
Code Multipath (m)	< 2-3	< 2-3	< 2-3
Noise (mm)	< 1	< 1	< 1

TABLE VI: Stationary antenna error probability summary.

Stationary	$Pr\{HE \leq 1 \text{ m}\}$	$Pr\{VE \leq 3 \text{ m}\}$	$Pr\{\|\delta\mathbf{P}^e\| \leq 3 \text{ m}\}$
SF GPS SPS	56.16%	93.27%	89.89%
SF GPS VN	81.00%	91.23%	89.01%
DF GNSS OS	45.43%	95.30%	93.37%
SF GNSS VN	91.46%	92.60%	91.19%
F9P SBAS	99.59%	99.88%	99.87%

Eqn. (2.24) in [61]). In the local tangent frame, the coordinates of $\mathbf{P}^g$ and $\delta\mathbf{P}^g$ are indicated by N, E, and D subscripts.

Each of these metrics will be analyzed with respect to the following standards: $Pr\{HE \leq 1 \text{ m}\}$, $Pr\{VE \leq 3 \text{ m}\}$, and $Pr\{\|\delta\mathbf{P}^e\| \leq 3 \text{ m}\}$, where $Pr\{x \leq \tau\}$ denotes the probability that x is less than threshold τ. Note that the SAE standards [1] require that $Pr\{HE \leq 1.5 \text{ m}\} \geq 68\%$ and $Pr\{VE \leq 3 \text{ m}\} \geq 68\%$.

E. Stationary Test Results

The experiment uses the receiver configurations labeled: SF GPS SPS, SF GPS VN, DF GNSS OS, SF GNSS VN, and F9P SBAS.

The test period is about 12 hours, with approximately 4.3×10^3 measurement epochs. Fig. 2 displays the cumulative error probability distributions for the error metrics defined in Section VI-D. The temporal error plots are also available (see Footnote 5). The statistics are summarized in Table VI. Table VI and Fig. 2 allow the following conclusions for the stationary data:

- SBAS performs the best with at least a 4-8% advantage in all the metrics. Note that this service is only available to users with SBAS capable receivers in the SBAS coverage area (e.g., WAAS for GPS in North America, EGNOS for Galileo in Europe, and BDSBAS for BeiDou in China).
- SF GPS VN and SF GNSS VN both yield significantly better horizontal accuracy than SF GPS SPS or DF GNSS OS. The VN-DGNSS approach improves the horizontal sub-meter level accuracy by 24.84% relative to SF GPS SPS and 46.03% relative to DF GNSS OS.
- All the configurations have vertical performance surpassing the SAE specification. F9P SBAS performs the best at all accuracy levels. DF GNSS OS performs second best. Vertical errors are significantly affected by atmospheric delays, which are best accommodated by two-frequency processing or, for users in N. America, the high-precision atmospheric model in WAAS. Fig. 2(b) shows SF GNSS VN performance approaches that of DF GNSS OS at smaller error levels.

F. Moving Test Results

Two experiments were performed over distinct time intervals using two u-blox antennae as follows:

1) The SF GNSS OS, SF GNSS VN, and F9P SBAS receiver configurations were performed using a single-band u-blox antenna.
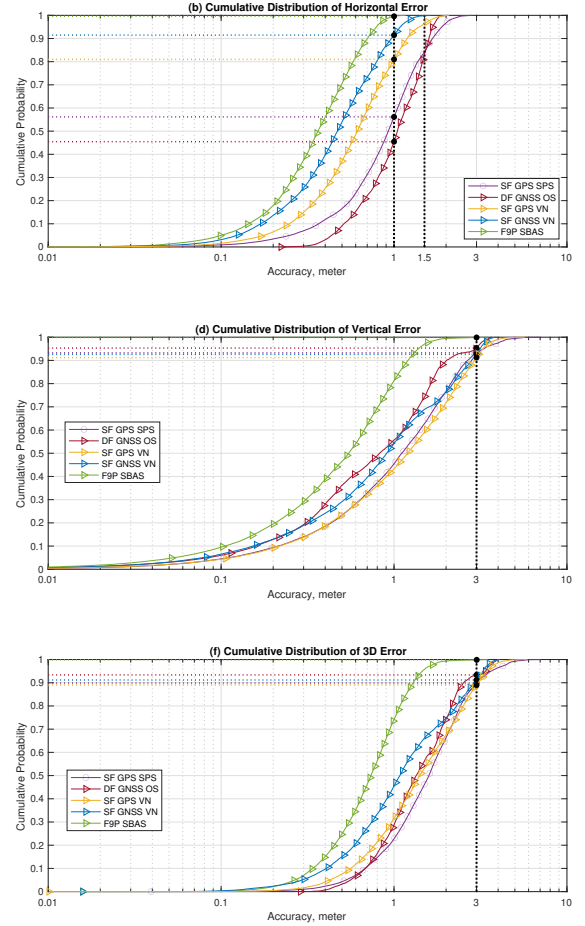

Fig. 2: Stationary experimental results. Subplots (a), (b), and (c) show the cumulative error distributions for the horizontal, vertical, and 3D position error metrics: blue for SF GPS SPS, orange for DF GNSS OS, green for SF GPS VN, purple for SF GNSS VN, and yellow for F9P SBAS.

2) The DF GNSS OS, SF GNSS VN, and F9P SBAS receiver configurations were performed using a dual-band u-blox antenna.

For the test using a single-band antenna experiment, the summary in Table VII shows that the SF GNSS VN and F9P SBAS configurations both surpass the SAE specifications for both horizontal and vertical accuracy. Both also surpass the 1m horizontal accuracy at 95% specification stated in Table 1 of [3] for Lane-Level applications. Both SF GNSS VN and F9P SBAS improve horizontal sub-meter level accuracy by 13.47% relative to SF GNSS OS. Fig. 3(b) shows that SF GNSS VN has better horizontal performance than SF GNSS OS and F9P SBAS at all accuracy levels. Fig. 3(d) shows that F9P SBAS achieved better vertical accuracy than SF GNSS VN, with the SF GNSS OS vertical performance failing to achieve the SAE specification.

TABLE VII: SF, moving platform, error summary.

Moving SF	$Pr\{HE \leq 1$ m$\}$	$Pr\{VE \leq 3$ m$\}$	$Pr\{\|\delta\mathbf{P}^e\| \leq 3$ m$\}$
SF GNSS OS	86.53%	0.00%	0.00%
SF GNSS VN	100.00%	100.00%	100.00%
F9P SBAS	100.00%	100.00%	100.00%

TABLE VIII: DF, moving platform, error summary.

Moving DF	$Pr\{HE \leq 1$ m$\}$	$Pr\{VE \leq 3$ m$\}$	$Pr\{\|\delta\mathbf{P}^e\| \leq 3$ m$\}$
DF GNSS OS	39.14%	93.82%	97.65%
SF GNSS VN	97.86%	100.00%	100.00%
F9P SBAS	96.30%	100.00%	100.00%

For the test using a dual-band antenna experiment, Fig. 4 and Table VIII show that SF GNSS VN and F9P SBAS achieve comparable performance which is significantly better than DF GNSS OS by greater than 55%. Fig. 4(d) shows that all three configurations surpass the SAE vertical accuracy specification. F9P SBAS achieves the best vertical accuracy, while SF GNSS VN surpasses DF GNSS OS.

VII. DISCUSSION

Table V predicts that multipath and ionospheric delay error will be the two largest remaining ranging errors. These predictions are supported by the reported experiments.

The effects of multipath are distinct for stationary and moving receivers. Multipath is caused by nearby reflective surfaces. For stationary antennae and reflectors, multipath can be correlated over long periods of time. For a moving platform, the receiver moves relative to the reflective surface; therefore, the multipath errors change much more rapidly (i.e., less correlated across time), which makes them easier for the receiver to filter out during the vehicle state estimation process. This is one explanation for the improved horizontal performance for the moving platform relative to the stationary platform.

Because the sign of the L1/E1/B1 code measurement ionospheric delay term is always positive, and the signs of the coefficients are always positive in the measurement observation matrix for the clock and Down-position components, the atmospheric delay most strongly contributes to error in the clock and Down estimates. Figures 2(d), 3(d), and 4(d) clearly show that SBAS (i.e., WAAS) achieves the best vertical accuracy. The WAAS performance analysis report [62] does not provide explicit assessment for WAAS ionosphere correction, but list the position horizontal and vertical errors as less than 1m at 95% for most sites in the continental United States. These performance levels imply that the WAAS ionosphere grid based model, which was originally designed for avionics applications within North America, achieves more accurate ionospheric delay predictions in southern California than does the CNES VTEC spherical harmonic model, which was designed for a global scale.

VIII. CONCLUSIONS AND FUTURE RESEARCH

This paper presents, demonstrates, and evaluates a VN-DGNSS approach that is built on a client-server architecture.

Usage of the server is free. The source code is available via open-source at the GitHub repository described in footnote 1. The VN-DGNSS server transmits RTCM OSR messages computed from real-time SSR data sources. RTCM SC-104 is a standard that defines the data structure for OSR differential correction information supported universally by almost all GNSS receivers.

The single-frequency code-measurement-only experiments presented in Sections VI-E and VI-F demonstrate that the VN-DGNSS succeeds in improving positioning accuracy relative to GNSS OS, without the user needing a physical base station near the user. The position estimation performance is comparable to that achieved using WAAS, but is available globally. This is valuable to users of RTCM enabled receivers that are not SBAS enable or that are operating in a region of the world not covered by an SBAS implementation.

There are several directions that could be considered for future research. This paper and the currently implemented system focus on single-frequency code measurements for navigation systems using CDMA. The extension to GLONASS, which uses FDMA, is more challenging. As discussed in Sect. 21.1.1 in [8] and footnote 2, there will be frequency-dependent biases between FDMA receiver's channels, that are different between receivers and are unknown. The VN-DGNSS approach could be extended to correct for GLONASS satellite orbit and clock errors, satellite code bias, satellite frequency dependent biases, and atmospheric errors. However, this would leave the receiver FDMA ICBs as significant sources of error. Extensions to multi-frequency and phase measurements are both interesting. The approach described herein can be extended to multiple frequencies per system; however, the scope of the funded project was limited to formulation and demonstration of the single frequency approach. For phase-measurement-based positioning, namely RTK, which is supported by many GNSS receivers. Sec. IV-E discusses the basic reasons why phase measurements are not currently supported by the VN-DGNSS for RTK. Precise Point Positioning Ambiguity Resolution (PPP-AR) using SSR products is a very active area of research [29], [63], [64] achieving centimeter to decimeter accuracy. A VN-DGNSS approach that packages the SSR products as OSR RTCM messages should be able to achieve these same accuracies using PPP-like methods. Research into such approaches is ongoing.

ACKNOWLEDGMENTS

REFERENCES

[1] "On-Board System Requirements for V2V Safety Communications J2945/1_201603," *Society of Automotive Engineers*, 2016.

[2] A. Vu, A. Ramanandan, A. Chen, J. A. Farrell, and M. Barth, "Real-Time Computer Vision/DGPS-Aided Inertial Navigation System for Lane-Level Vehicle Navigation," *IEEE Trans. Intell. Transp. Syst.*, vol. 13, no. 2, pp. 899–913, 2012.
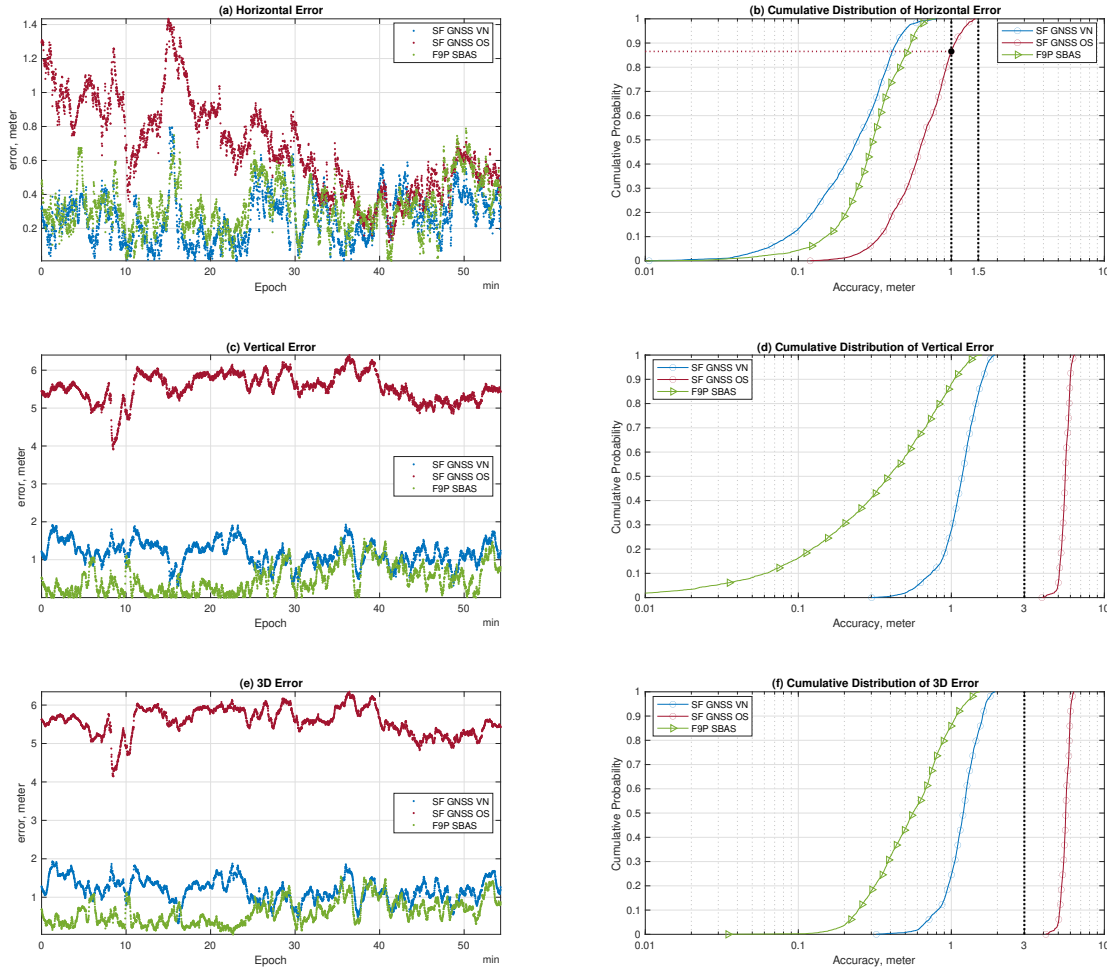
Fig. 3: Experimental results for a moving platform test using a single-band antenna. Subplots (a), (c), and (e) show the horizontal, vertical, and 3D position error plotted versus time. The *x*-axis is the epoch number. Subplots (b), (d), and (f) show the cumulative error distribution of the horizontal, vertical, and 3D position error metrics: blue for SF GNSS VN, red for SF GNSS OS, and green for F9P SBAS.

[3] N. Williams and M. Barth, "A qualitative analysis of vehicle positioning requirements for connected vehicle applications," *IEEE Intell. Transp. Syst. Mag.*, vol. 13, no. 1, pp. 225–242, 2021.

[4] K. Boriboonsomsin, M. J. Barth, W. Zhu, and A. Vu, "Eco-routing navigation system based on multisource historical and real-time traffic information," *IEEE Trans. Intell. Transp. Syst.*, vol. 13, no. 4, pp. 1694–1704, 2012.

[5] G. P. Team, "Global positioning system standard positioning service performance analysis report," *GPS Product Team: Washington, DC, USA*, 2020.

[6] "BeiDou navigation satellite system open service performance standard (Version 2.0)," *China Satellite Navigation Office*, 2018.

[7] "European GNSS (Galileo) open service service definition document," *European GNSS Service Centre*, 2019.

[8] P. Teunissen and O. Montenbruck, *Springer handbook of global navigation satellite systems*. Springer, 2017.

[9] F. Rahman, F. Silva, Z. Jiang, and J. A. Farrell, "ECEF position accuracy and reliability: Continent scale differential GNSS approaches (Phase C report)," *https://escholarship.org/uc/item/05p9p3c9*, 2019.

[10] X. Chen, T. Allison, W. Cao, K. Ferguson, S. Grunig, V. Gomez, A. Kipka, J. Kohler, H. Landau, R. Leandro *et al.*, "Trimble RTX, an innovative new approach for network RTK," in *Proc. of the 24th international technical meeting of the satellite division of the institute of navigation*, 2011, pp. 2214–2219.

[11] U. Vollath, A. Buecherl, H. Landau, C. Pagels, and B. Wagner, "Multi-base RTK positioning using virtual reference stations," in *Proc. of the 13th International Technical Meeting of the Satellite Division of The Institute of Navigation*, 2000, pp. 123–131.

[12] L. Wanninger, "Real-time differential GPS error modelling in regional reference station networks," in *Advances in positioning and reference frames*. Springer, 1998, pp. 86–92.

[13] Trimble VRS Coverage, https://positioningservices.trimble.com/resources/coverage-maps-3/.

[14] OmniSTAR VBS, https://www.omnistar.com/subscription-services/omnistar-vbs/.

[15] Qianxun SI FindM, https://www.qxwz.com/en/products.

[16] "Global positioning systems directorate system engineering & integration interface specification IS-GPS-200H," *Navstar GPS Space Segment/Navigation User Interfaces*, 2013.

[17] "Galileo signal in space interface control document (OS SIS ICD)," *Galileo Open Service*, 2008.

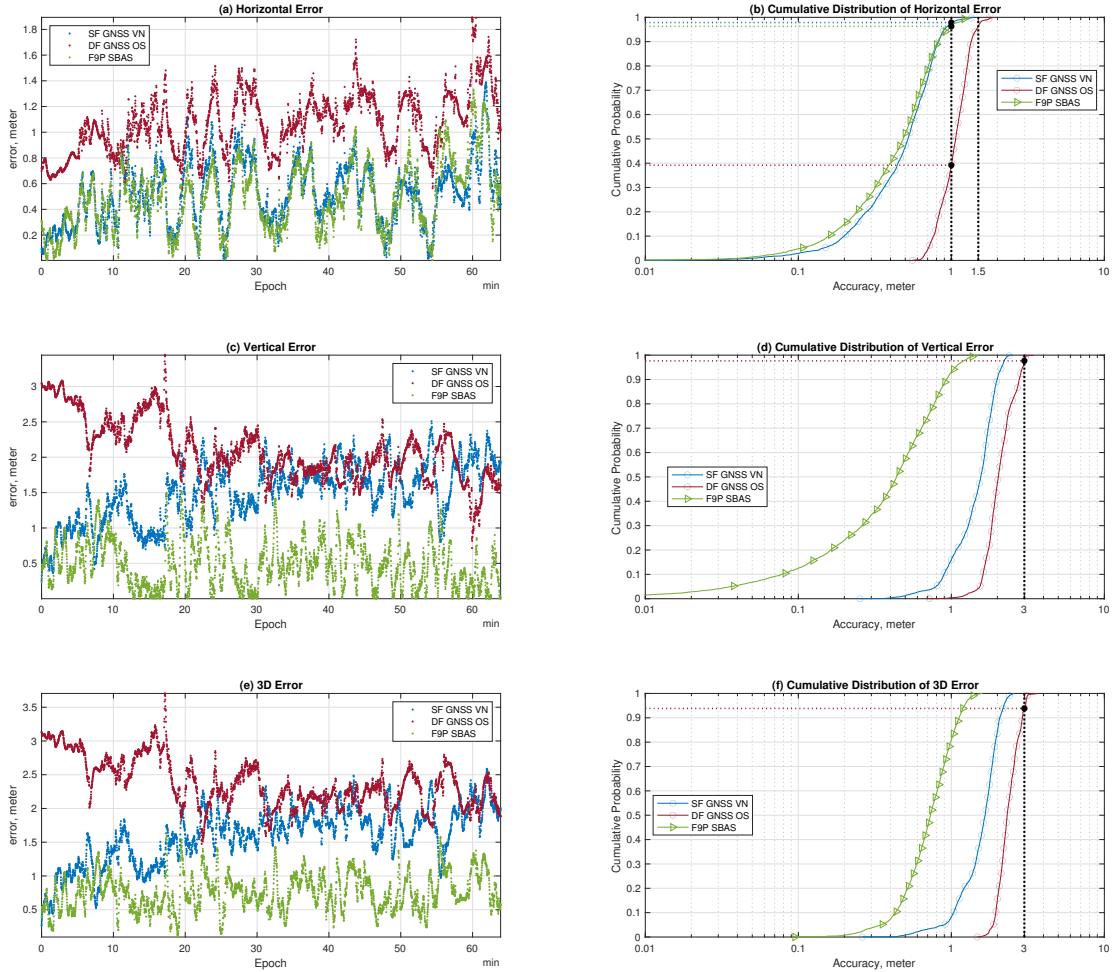[18] "BeiDou navigation satellite system signal in space interface control

Fig. 4: Experimental results for a moving platform test using a dual-band antenna. Subplots (a), (c), and (e) show the horizontal, vertical, and 3D position error plotted versus time. The *x*-axis is the epoch number. Subplots (b), (d), and (f) show the cumulative error distribution of the horizontal, vertical, and 3D metrics: blue for SF GNSS VN; red for DF GNSS OS; and green for F9P SBAS.

document open service signal B1I (Version 3.0)," *China Satellite Navigation Office*, 2019.

[19] "Glonass interface control document," *Russian Institute of Space Device Engineering: Moscow, Russia*, 2008.

[20] W. Song, W. Yi, Y. Lou, C. Shi, Y. Yao, Y. Liu, Y. Mao, and Y. Xiang, "Impact of GLONASS pseudorange inter-channel biases on satellite clock corrections," *GPS Solutions*, vol. 18, no. 3, pp. 323–333, 2014.

[21] L. Wanninger, "Carrier-phase inter-frequency biases of GLONASS receivers," *J. of Geodesy*, vol. 86, no. 2, pp. 139–148, 2012.

[22] W. Hu and J. A. Farrell, "Derivation of earth-rotation correction (Sagnac) and analysis of the effect of receiver clock bias," *https://escholarship.org/uc/item/1bf6w7j5*, 2019.

[23] B. Stressler, J. Heck, and H. Steve, "An assessment of the accuracy of broadcast ephemerides for multi-GNSS positioning," in *IGS workshop*, 2018.

[24] J. Geng, X. Chen, Y. Pan, and Q. Zhao, "A modified lock/bias model to improve PPP ambiguity resolution at Wuhan University," *J. of Geodesy*, vol. 93, no. 10, pp. 2053–2067, 2019.

[25] N. Wang, Y. Yuan, Z. Li, O. Montenbruck, and B. Tan, "Determination of differential code biases with multi-GNSS observations," *J. of Geodesy*, vol. 90, no. 3, pp. 209–228, 2016.

[26] O. Montenbruck, A. Hauschild, and P. Steigenberger, "Differential code bias estimation using multi-GNSS observations and global ionosphere maps," *J. of the Inst. of Navigation*, vol. 61, no. 3, pp. 191–201, 2014.

[27] O. Bock and E. Doerflinger, "Atmospheric modeling in GPS data analysis for high accuracy positioning," *Physics and Chemistry of the Earth, Part A*, vol. 26, no. 6-8, pp. 373–383, 2001.

[28] J. A. Farrell, *Aided navigation: GPS with high rate sensors*. McGraw-Hill, Inc., 2008.

[29] D. Laurichesse, F. Mercier, and J.-P. Berthias, "Real-time PPP with undifferenced integer ambiguity resolution, experimental results," in *Proc. of the 23rd International Technical Meeting of The Satellite Division of the Institute of Navigation*, 2010, pp. 2534–2544.

[30] "IGS state space representation (SSR) format version 1.00," *IGS Real-Time Working Group*, 2020.

[31] T. Hadas and J. Bosy, "IGS RTS precise orbits and clocks verification and quality degradation over time," *GPS Solutions*, vol. 19, no. 1, pp. 93–105, 2015.

[32] E. Sardon, A. Rius, and N. Zarraoa, "Estimation of the transmitter and receiver differential biases and the ionospheric total electron content from Global Positioning System observations," *Radio Science*, vol. 29, no. 03, pp. 577–586, 1994.

[33] J. Ray and K. Senior, "Geodetic techniques for time and frequency comparisons using GPS phase and code measurements," *Metrologia*, vol. 42, no. 4, p. 215, 2005.

[34] S. Schaer, "SINEX BIAS—Solution (Software/technique) independent exchange format for GNSS biases version 1.00," in *IGS Workshop on GNSS Biases, Bern, Switzerland*, 2016.

[35] N. Wang, Z. Li, B. Duan, U. Hugentobler, and L. Wang, "GPS and GLONASS observable-specific code bias estimation: comparison of solutions from the IGS and MGEX networks," *J. of Geodesy*, vol. 94, no. 8, pp. 1–15, 2020.

[36] R. Leandro, M. Santos, and R. Langley, "Unb neutral atmosphere models: development and performance," in *Proc. of the National Technical Meeting of The Institute of Navigation*, 2006, pp. 564–573.

[37] W. Li, Y. Yuan, J. Ou, H. Li, and Z. Li, "A new global zenith tropospheric delay model IGGtrop for GNSS applications," *Chinese Science Bulletin*, vol. 57, no. 17, pp. 2132–2139, 2012.

[38] K. Kazmierski, M. Santos, and J. Bosy, "Tropospheric delay modelling for the EGNOS augmentation system," *Survey Review*, vol. 49, no. 357, pp. 399–407, 2017.

[39] N. Penna, A. Dodson, and W. Chen, "Assessment of EGNOS tropospheric correction model," *J. of Navigation*, vol. 54, pp. 37 – 55, 01 2001.

[40] W. Li, Y. Yuan, J. Ou, Y. Chai, Z. Li, Y.-A. Liou, and N. Wang, "New versions of the BDS/GNSS zenith tropospheric delay model IGGtrop," *J. of Geodesy*, vol. 89, no. 1, pp. 73–80, 2015.

[41] W. Li, Y. Yuan, J. Ou, and Y. He, "IGGtrop_SH and IGGtrop_rH: Two improved empirical tropospheric delay models based on vertical reduction functions," *IEEE Trans. Geosci. Remote Sens.*, vol. 56, no. 9, pp. 5276–5288, 2018.

[42] J. A. Klobuchar, "Ionospheric time-delay algorithm for single-frequency GPS users," *IEEE Trans. Aerosp. Electron. Syst.*, no. 3, pp. 325–331, 1987.

[43] "Ionospheric correction algorithm for Galileo single frequency users (V1.2)," *European GNSS Service Centre*, 2016.

[44] Y. Yuan, X. Huo, J. Ou, K. Zhang, Y. Chai, D. Wen, and R. Grenfell, "Refining the Klobuchar ionospheric coefficients based on GPS observations," *IEEE Trans. Aerosp. Electron. Syst.*, vol. 44, no. 4, pp. 1498–1510, 2008.

[45] A. Angrisano, S. Gaglione, C. Gioia, M. Massaro, and U. Robustelli, "Assessment of NeQuick ionospheric model for Galileo single-frequency users," *Acta Geophysica*, vol. 61, no. 6, pp. 1457–1476, 2013.

[46] R. S. Committee *et al.*, "Proposal of new RTCM SSR messages, SSR stage 2: Vertical TEC (VTEC) for RTCM standard 10403.2 differential GNSS (Global Navigation Satellite Systems) services-version 3," *RTCM Special Committee*, no. 104, 2014.

[47] Z. Li, N. Wang, M. Hernandez-Pajares, Y. Yuan, A. Krankowski, A. Liu, J. Zha, A. Garcia-Rigo, D. Roma-Dollase, H. Yang *et al.*, "IGS real-time service for global ionospheric total electron content modeling," *J. of Geodesy*, vol. 94, no. 3, pp. 1–16, 2020.

[48] Z. Li, Y. Yuan, N. Wang, M. Hernandez-Pajares, and X. Huo, "SHPTS: Towards a new method for generating precise global ionospheric TEC map based on spherical harmonic and generalized trigonometric series functions," *J. of Geodesy*, vol. 89, no. 4, pp. 331–345, 2015.

[49] D. Laurichesse and A. Blot, *New CNES real time products including BeiDou*. IGS Mail No. 7183, 10 Nov 2015.

[50] T. Fuller-Rowell, "USTEC: a new product from the space environment center characterizing the ionospheric total electron content," *GPS Solutions*, vol. 9, no. 3, pp. 236–239, 2005.

[51] USTEC Real-time TEC, https://services.swpc.noaa.gov/text/us-tec-total-electron-content.txt.

[52] M. B. El-Arini, P. A. O'Donnell, P. M. Kellam, J. A. Klobuchar, T. C. Wisser, and P. H. Doherty, "The FAA wide area differential GPS (WADGPS) static ionospheric experiment," in *Proc. of the National Technical Meeting of the Institute of Navigation*, 1993, pp. 485–496.

[53] F. D. S. Prol, P. D. O. Camargo, and M. T. D. A. H. Muella, "Comparative study of methods for calculating ionospheric points and describing the GNSS signal path," *Boletim de Ciências Geodésicas*, vol. 23, no. 4, pp. 669–683, 2017.

[54] M. L. Psiaki and S. Mohiuddin, "Modeling, analysis, and simulaiton of GPS carrier phase for spacecraft relative navigation," *J. of Guidance, Control, and Dynamics*, vol. 30, no. 6, pp. 1682–1639, 2007.

[55] G. Weber, L. Mervart, and A. Stürze, *BKG Ntrip Client (BNC): Version 2.12*. Verlag des Bundesamtes für Kartographie und Geodäsie, 2016.

[56] T. Takasu and A. Yasuda, RTKLIB Repository: https://github.com/tomojitakasu/RTKLIB.

[57] T. Takasu and A. Yasuda, "Development of the low-cost RTK-GPS receiver with an open source program package RTKLIB," *Int. Symposium on GPS/GNSS*, vol. 1, 2009.

[58] The PPP-Wizard project of CNES, http://www.ppp-wizard.net/news.html.

[59] Z. Wang, Z. Li, L. Wang, X. Wang, and H. Yuan, "Assessment of multiple GNSS real-time SSR products from different analysis centers," *ISPRS Int. Journal of Geo-information*, vol. 7, no. 3, p. 85, 2018.

[60] N. Wang, Z. Li, and Y. Yuan, "Multi-GNSS code bias handling: an observation specific perspective," in *IGS workshop*, 2018.

[61] G. Cai, B. M. Chen, and T. H. Lee, *Unmanned rotorcraft systems*. Springer Science & Business Media, 2011.

[62] "Wide area augmentation system performance analysis report," *nstb.tc.faa.gov*, 2020.

[63] J. Geng, X. Chen, Y. Pan, S. Mao, C. Li, J. Zhou, and K. Zhang, "PRIDE PPP-AR: An open-source software for GPS PPP ambiguity resolution," *GPS Solutions*, vol. 23, no. 4, p. 91, 2019.

[64] X. Li, X. Li, Y. Yuan, K. Zhang, X. Zhang, and J. Wickert, "Multi-GNSS phase delay estimation and PPP ambiguity resolution: GPS, BDS, GLONASS, Galileo," *J. of Geodesy*, vol. 92, no. 6, pp. 579–608, 2018.
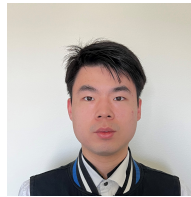
Wang Hu received the B.S. degree in electronics and information engineering from North China Electric Power University, Beijing, China. He is pursuing his Ph.D. degree in Electrical and Computer Engineering in University of California, Riverside, CA, USA. His research interests include automated driving, GNSS, aided inertial navigation, state estimation.

Ashim Neupane received the B.S. degree in mechanical engineering from Howard University, Washington, D.C., USA. He is pursuing his Ph.D. degree in Electrical and Computer Engineering in University of California, Riverside, CA, USA. His research interests include navigation, state estimation, robotics and controls.

Jay A. Farrell received the B.S. degrees in physics and electrical engineering from Iowa State University, Ames, IA, USA, and the M.S. and Ph.D. degrees in electrical engineering from the University of Notre Dame, Notre Dame, IN, USA. After working at Charles Stark Draper Lab (1989–1994), he joined the University of California, Riverside, CA, USA, where he is the KA Endowed Chair in the Department of Electrical and Computer Engineering. He has authored over 250 technical articles and three books. He was named a GNSS Leader to Watch for 2009–2010 by GPS World Magazine in May 2009. He was General Chair for IEEE CDC 2012 and has served the IEEE Control Systems Society and the American Association of Automatic Control as President. Prof. Farrell is a Distinguished Member of IEEE CSS and a Fellow of the IEEE, IFAC, and AAAS.

APPENDIX

The following material is included for the benefit of the reviewers only. It would not appear in the published version.

A. Derivation of Partial Derivative

The objective of this section is to derive Eqn. (6).

For the error function $F(t_p^s)$ defined in Eqn. (5), the partial derivative is evaluated as follows:

$$\frac{\partial F}{\partial t_p^s} = \frac{\partial}{\partial t_p^s} \left(R\left(\mathbf{P}_b, \hat{\mathbf{P}}^s(t_b - t_g^s) \right) - c t_g^s \right)$$

$$= \left(\frac{\partial}{\partial t_g^s} R\left(\mathbf{P}_b, \hat{\mathbf{P}}^s(t_b - t_g^s) \right) - c \right) \frac{\partial t_g^s}{\partial t_p^s}$$

$$= -\left(\frac{\partial}{\partial \mathbf{P}^s} R\left(\mathbf{P}_b, \mathbf{P}^s \right) \bigg|_{\mathbf{P}^s = \hat{\mathbf{P}}^s(t_b - t_g^s)} \frac{\partial \mathbf{P}^s}{\partial t} \bigg|_{t = t_b - t_g^s} + c \right) \frac{\partial t_g^s}{\partial t_p^s}$$

where $\mathbf{1}_b^s = \frac{\partial}{\partial \mathbf{P}^s} R\left(\mathbf{P}_b, \mathbf{P}^s \right) \bigg|_{\mathbf{P}^s = \hat{\mathbf{P}}^s(t_b - t_p^s)}$ is a unit vector and

$$\hat{\mathbf{V}}^s(t_b - t_p^s) = \frac{\partial \mathbf{P}^s}{\partial t} \bigg|_{t = t_b - t_p^s}.$$

Given that $t_g^s = t_p^s + \hat{dt}^s(\hat{t}^s)$ and $\hat{t}^s = t_b - t_p^s$,

$$\frac{\partial t_g^s}{\partial t_p^s} = 1 + \frac{\partial \hat{dt}^s(\hat{t}^s)}{\partial t_p^s} \tag{26}$$

$$= 1 + \left(\frac{\partial}{\partial \hat{t}^s} \hat{dt}^s(\hat{t}^s) \right) \left(\frac{\partial \hat{t}^s}{\partial t_p^s} \right) \tag{27}$$

$$= \left(1 - \frac{\partial}{\partial \hat{t}^s} \hat{dt}^s(\hat{t}^s) \right) \tag{28}$$

$$= \left(1 - (a_1 + 2 a_2 (\hat{t}^s - t_{oc})) \right), \tag{29}$$

where a_1, a_2, and t_{oc} are the clock model parameters from the navigation message. Therefore,

$$\frac{\partial F}{\partial t_p^s} = -\left(\mathbf{1}_b^s \cdot \hat{\mathbf{V}}^s(t_b + t_g^s) + c \right) \left(1 - a_1 - 2 a_2 (\hat{t}^s - t_{oc}) \right).$$